Acta Polytechnica **55**(1):34–38, 2015
doi:10.14311/AP.2015.55.0034

available online at http://ojs.cvut.cz/ojs/index.php/ap

OPERATION MODES AND CHARACTERISTICS OF A PLASMA DIPOLE ANTENNA

Nikolay N. Bogachev[a,b,*], Irina L. Bogdankevich[b,c], Namik G. Gusein-zade[b,c], Konstantin F. Sergeychev[b]

[a] *Moscow State Technical University of Radio Engineering, Electronics and Automation, Moscow, Russia*

[b] *Prokhorov General Physics Institute, Russian Academy of Sciences, Moscow, Russia*

[c] *Pirogov Russian National Research Medical University, Moscow, Russia*

[*] corresponding author: bgniknik@yandex.ru

Abstract. The existence modes of a surface electromagnetic wave on a plasma cylinder, and the operating modes and characteristics of a plasma antenna are studied in this paper. Solutions of the dispersion equation of the surface wave are obtained for a plasma cylinder of finite radius for different plasma density values. The operation modes of a plasma asymmetric dipole antenna of finite length and radius are researched by numerical simulation. The electric field distributions of the plasma antenna in the near field and the radiation pattern are obtained. These characteristics are compared with the characteristics of a similar metal antenna. Numerical models are verified by comparing the counted and measured metal antenna radiation patterns.

Keywords: plasma antenna, surface electromagnetic wave, numerical simulation, operation modes, metal monopole, radiation pattern.

1. Introduction

In recent years much plasma antenna research has been done by theoretical, numerical and experimental methods [1–11]. The most popular plasma antenna type is the Plasma Asymmetrical Dipole (monopole) antenna (PAD) [1, 2, 4–11]. Some little explored problems of plasma antennas are: the noise performances of the plasma antenna; non-linear distortions and current instabilities in the plasma of gas discharge, the choice of optimum plasma parameters for PAD operation, and the role of the surface electromagnetic wave (surface wave) [12] in antenna operation. Our research was focused on the determining the influence of plasma density on the radiation modes of PAD and the interrelation surface wave with antenna operation modes.

Previous papers [2, 4, 5, 8–11] have reported numerical simulation results. In the context of the simulations, some characteristics of plasma antennas have been determined. In these simulations such plasma density values n_e were used that plasma antenna functioned like metal antenna ($\omega_{Pe} > 10 \cdot \omega_{ew0}$). However, in experimental studies the plasma density values may be very different, and the plasma frequency may be close to the threshold $\omega_{Pe} \approx \sqrt{2}\,\omega_{ew0}$. In this case, the radiation antenna fails, or nonlinear distortions appear in the transmitted signal. For example, it was shown in [7] that at a frequency of 400 MHz, the radiated power dependence $P(n_e)$ represents a nonlinear function. Our task was to study the interrelation between the surface electromagnetic wave and the operation modes of a plasma antenna for plasma frequency values in the range of $\sqrt{2}\,\omega_{ew0} \le \omega_{Pe} \le 15 \cdot \omega_{ew0}$, where $\omega_{ew0} = 2\pi f_0 = 2\pi \cdot 1.7\,\text{GHz} = 1.07 \cdot 10^{10}\,\text{rad/s}$.

2. Surface electromagnetic wave on a cylindrical plasma column

We will consider in this section distribution conditions of the existence modes of a surface electromagnetic wave on the boundary of a plasma cylinder of infinite length and fixed radius r_0. For this, we use the dispersion equation for an azimuthal symmetric surface wave on the cylindrical surface of a conducting medium of radius r_0 [13]:

$$\varepsilon\sqrt{{k_z}^2 - \frac{\omega_{ew}^2}{c^2}}\,\frac{K_0\left(\sqrt{{k_z}^2 - \frac{\omega_{ew}^2}{c^2}}\,r_0\right)}{K_0'\left(\sqrt{{k_z}^2 - \frac{\omega_{ew}^2}{c^2}}\,r_0\right)} - \sqrt{{k_z}^2 - \frac{\omega_{ew}^2}{c^2}\varepsilon}\,\frac{I_0\left(\sqrt{{k_z}^2 - \frac{\omega_{ew}^2}{c^2}\varepsilon}\,r_0\right)}{I_0'\left(\sqrt{{k_z}^2 - \frac{\omega_{ew}^2}{c^2}\varepsilon}\,r_0\right)} = 0, \quad (1)$$

where plasma dielectric permittivity ε is defined as

$$\varepsilon(\omega) = \varepsilon_0 - \frac{\omega_{Pe}^2}{\omega_{ew}\left(\omega_{ew} + i\,\nu_e\right)} = \begin{cases} \varepsilon_0 - \dfrac{\omega_{Pe}^2}{\nu_e^2} + i\,\dfrac{\omega_{Pe}^2}{\omega_{ew}\,\nu_e} & \text{if } \omega_{ew} \ll \nu_e, \\ \varepsilon_0 - \dfrac{\omega_{Pe}^2}{\omega_{ew}^2}\left(1 - i\,\dfrac{\nu_e}{\omega_{ew}}\right) & \text{if } \omega_{ew} \gg \nu_e, \end{cases} \quad (2)$$

and $\omega_{Pe} = \sqrt{n_e e^2/m_e\varepsilon_0}$ — electron plasma frequency, I_0, K_0 and I_0', K_0' — modified Bessel functions and their derivatives respectively, k_z — a wave number, $\omega_{ew} = 2\pi f$ — the cyclic frequency of an electromagnetic wave, c — velocity of light, ν_e — electron colli-

sion frequency, ε_0 — relationship dielectric permittivity, n_e — electron plasma density, m_e and e — mass and charge of an electron.

The real part of the solution of the dispersion equation (1) is given in Fig. 1 for the parameters of the plasma used in the simulation part of our studies. Note that $\nu_e = 10^7\,\mathrm{s}^{-1}$, for argon in a tube with pressure $p_0 = 3\cdot 10^{-2}\,\mathrm{Torr} = 4\,\mathrm{Pa}$ [4], $r_0 = 0.5\,\mathrm{cm}$, and the angular frequency on the vertical axis of the graphs in Fig. 1 normalized $\omega = \frac{\omega_{ew}\, r_0}{c}$, so $\omega_0 = \frac{\omega_{ew0}\, r_0}{c} = 0.18$ and $k = k_z r_0$ Fig. 1,a shows for $\omega_{Pe} = \sqrt{2}\omega_{ew0} = 1.58\cdot 10^{10}\,\mathrm{rad/s}$ ($n_e = 8.0\cdot 10^{10}\,\mathrm{cm}^{-3}$) that frequency ω_0 misses the asymptotic part of the dispersion curve. In this case, the surface electromagnetic wave propagates along the plasma column and does not radiate into the surrounding space (nonradiative mode).

If $\omega_{Pe} = 5.35\cdot 10^{10}\,\mathrm{rad/s}$ ($n_e = 9.1\cdot 10^{11}\,\mathrm{cm}^{-3}$) (see Fig. 1,b) wave frequency ω_0 falls on the nonlinear part of the dispersion curve. At such settings, the electromagnetic wave radiated in space, although the emitted characteristics wave are suboptimal. In this sub-optimal (or transition) mode any small change in the wave parameters can lead to a change in the characteristics of the radiation.

For plasma $\omega_{Pe} = 1.07\cdot 10^{11}\,\mathrm{rad/s}$ ($n_e = 3.6\cdot 10^{12}\,\mathrm{cm}^{-3}$) (see Fig. 1,c), wave frequency ω_0 is near the border of the linear part and the radiation characteristics are close to optimal. This will be called the linear mode.

3. Model verification

In this section, we compare the results of numerical simulations and experimental measurements of the radiation pattern for verification. We investigated the Metal Asymmetric Dipole (monopole) antenna (MAD) with $l_a = 4.1cm$; $d_a = 0.3cm$; $D_s = 18cm$ at frequency $f_0 = 1.7GHz$. The radiation pattern in the far field of MAD was obtained by numerical simulation in KARAT code [14] and CAD EMpro [15] and experimental measurements were carried out in an anechoic chamber. The general scheme of the quarterwave asymmetric dipole with length l_a, diameter $d_a = 2R_a$ metal screen diameter $D_s = 2R_s$ is shown in Fig. 2.

The MAD model was implemented in full electromagnetic KARAT code [14] in the $2.5D$ version. We consider the axisymmetric case with a perfect matching layer (PML) on the borders of the counting area. The metal screen and the pin of MAD were given as perfectly conducting surface. Simulation was carried out by the finite difference time domain (FDTD) method.

The model in EMpro was created in three-dimensional geometry in the xyz coordinate system, with a resizable and perfect matching layer at the edges of the counting area. The calculation was performed using the finite element method (FEM) in the block Agilent FEM Simulator.

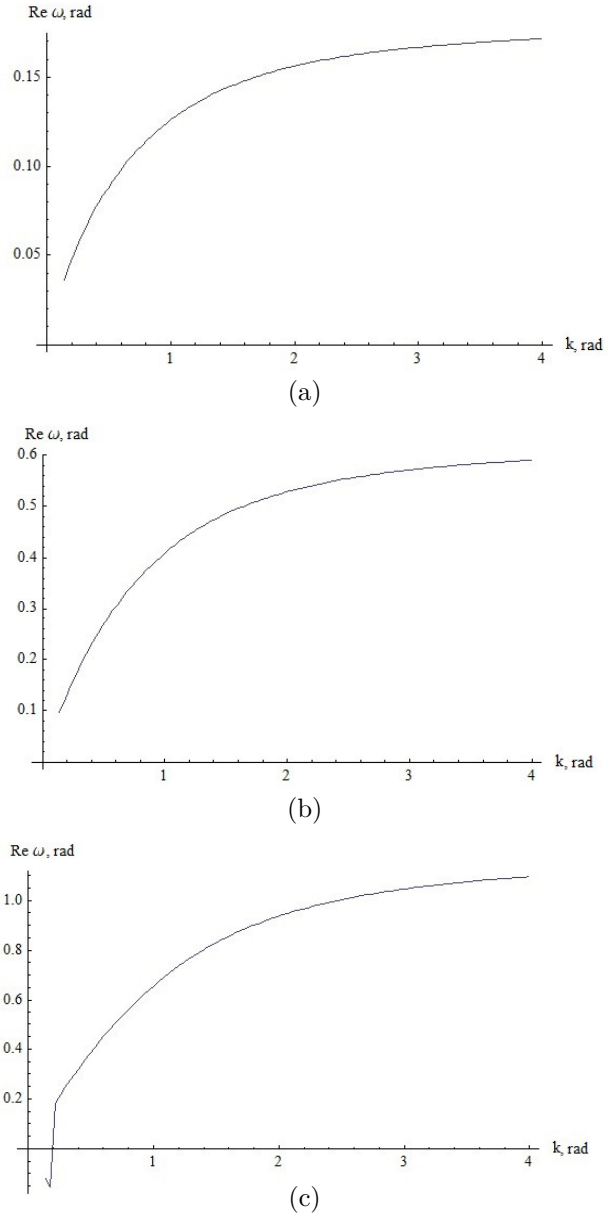

Figure 1. Real parts of dispersion equation solutions for plasma:
a) $\omega_{Pe} = 1.58\cdot 10^{10}\,\mathrm{rad/s}$ ($n_e = 8.0\cdot 10^{10}\,\mathrm{cm}^{-3}$),
b) $\omega_{Pe} = 5.35\cdot 10^{10}\,\mathrm{rad/s}$ ($n_e = 9.1\cdot 10^{11}\,\mathrm{cm}^{-3}$),
c) $\omega_{Pe} = 1.07\cdot 10^{11}\,\mathrm{rad/s}$ ($n_e = 3.6\cdot 10^{12}\,\mathrm{cm}^{-3}$).

Fig. 2 shows the results of a numerical simulation and measurement of the radiation patterns for MAD with $l_a = 4.1\,\mathrm{cm}$; $d_a = 0.3\,\mathrm{cm}$ and $D_s = 18\,\mathrm{cm}$ at the frequency $f_0 = 1.7\,\mathrm{GHz}$. As can be seen from the graphs, the radiation patterns coincide on the main lobe. The side lobes have differences in level and in position. The radiation pattern obtained in KARAT code differs from the measured radiation pattern because the absorber layer is very near to the back surface of the metal screen in the model. The differences in the radiation pattern of the EMPro model is due to the fact that the FEM method are not very correct for devices with a small Q-factor (gain–bandwidth) [15].

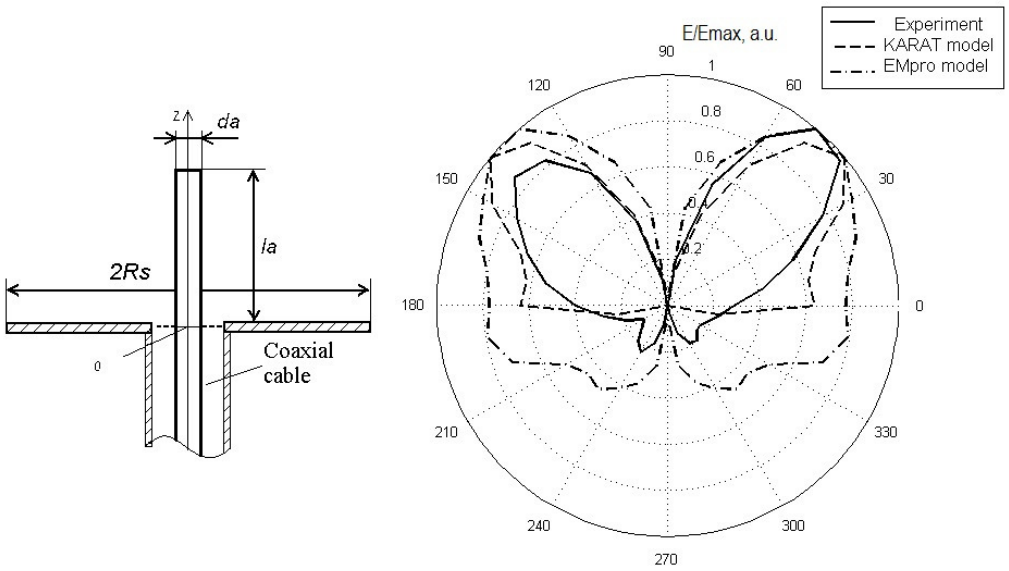

FIGURE 2. Scheme of an asymmetric dipole (monopole) antenna (left side) and the experimental and modeling radiation pattern (right side) of metal asymmetric dipole antenna.

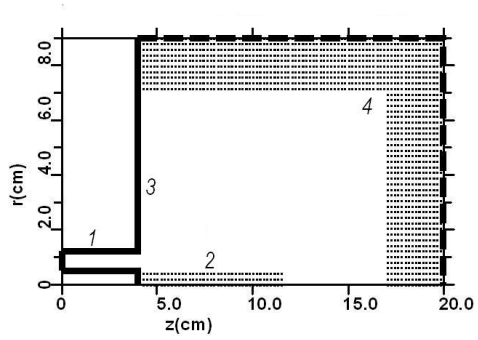

FIGURE 3. Plasma antenna model in KARAT code: 1 — coaxial cable, 2 — plasma column, 3 — metal screen, 4 — absorber (PML).

4. NUMERICAL SIMULATION RESULTS AND DISCUSSION

This section presents the results of a numerical simulation of the plasma and metal asymmetric dipole ($l_a = 4\,\text{cm}$, $d_a = 1\,\text{cm}$) with an infinite size of the screen $D_s = \infty$. The plasma in the model was set as the medium described by the Drude theory, where the dielectric permittivity of the plasma was determined by formula (3) [16]:

$$\varepsilon(\omega) = 1 - \frac{\omega_{Pe}^2}{\omega_{ew}\left(\omega_{ew} - i\nu_e\right)}, \qquad (3)$$

In this model (see Fig. 3.), the Gaussian pulse with $\tau_i = 15\,\text{ns}$ and frequency $f_0 = 1.7\,\text{GHz}$ reached the plasma (metal) antenna through a coaxial cable. The plasma parameters were changed by varying the plasma density n_e (the electron collision frequency remained constant $\nu_e = 10^7 s^{-1}$).

The field of the quarterwave dipole has structure of a TM-mode. So we consider the functions $E_z(r)$ and $E_r(z)$ to be the most informative. In addition, the selection function $E_r(z)$ is due to the proportionality of this component to the distribution of charge Q along the antenna. The spatial structure of the field components $E_z(r)$ and $E_r(z)$ (Fig. 4 and Fig. 5) was plotted for the plasma and metal antennas $l_a = 4\,\text{cm}$, $d_a = 1\,\text{cm}$, $D_s = \infty$ according to the simulation results of code KARAT at frequency $f_0 = 1.7\,\text{GHz}$.

No.	**Ratio** ω_p **vs** ω_{ew0} **vs** f_0	ω_p [rad/s]	n_e [cm^{-3}]
1	$\sqrt{2}\cdot\omega_{ew0} = \sqrt{2}\cdot 2\pi f_0$	$1.58\cdot 10^{10}$	$8.0\cdot 10^{10}$
2	$5\cdot\omega_{ew0} = 5\cdot 2\pi f_0$	$5.35\cdot 10^{10}$	$9.1\cdot 10^{11}$
3	$10\cdot\omega_{ew0} = 10\cdot 2\pi f_0$	$1.07\cdot 10^{11}$	$3.6\cdot 10^{12}$

TABLE 1. Parameters of the plasma.

In Fig. 4, function $E_r(z)$ are presented in the three operating modes of PAD. In the first mode (the parameters correspond to point No. 1 in Table 1) there is a surface wave distribution with wavelength $\lambda \approx 1.5\,\text{cm}$ along a plasma column of the antenna (curve 1). This wavelength matches the wavelength calculated in Section 2 for the same parameters. This case is a nonradiative mode. The second mode (No. 2 in Table 1) is suboptimal transition mode (curve 2). The third mode (No. 3 in Table 1) of the plasma antenna (curve 3) is close to the operation mode of the metal asymmetrical dipole (curve 4).

In Fig. 5, the graphics $E_z(r)$ are for the same plasma concentration values as in Fig. 4. Three qualitatively different operation modes of the plasma antenna are also clearly visible. In the first mode (curve 1), can be seen as $E_z(r)$ fades out in both directions from the boundaries of the plasma-vacuum at a different speed

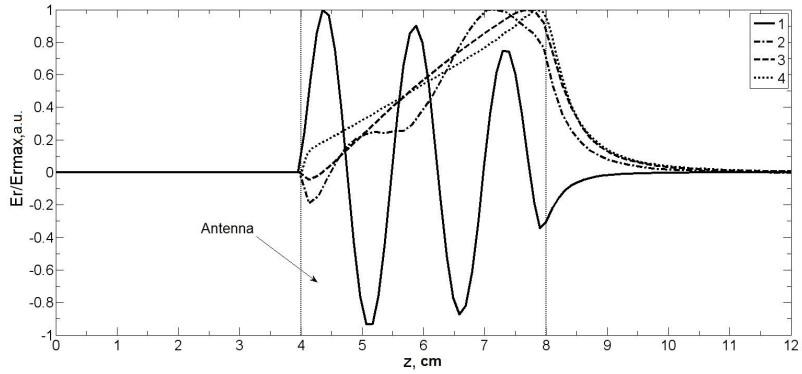

FIGURE 4. Distributions of $E_r(z)$: 1–3 — modes of the plasma antenna, 4 — the metal antenna.

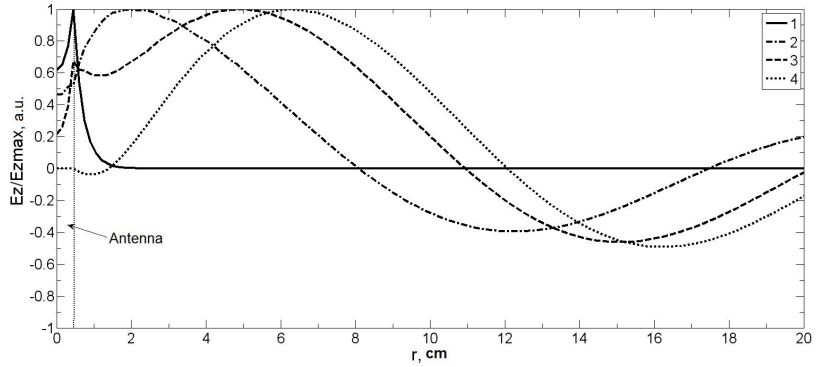

FIGURE 5. Distributions of $E_z(r)$: 1–3 — modes of the plasma antenna, 4 — the metal antenna.

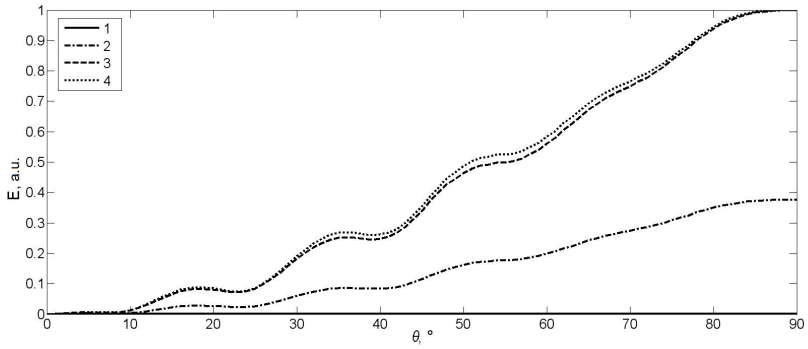

FIGURE 6. Radiation patterns: 1–3 — modes of the plasma antenna, 4 — the metal antenna.

and in a vacuum it fades out at the distance $a = 1cm$, which is much smaller than the wavelength supplied to the antenna ($\lambda \approx 18$ cm). This indicates that when $\omega_{Pe} = \sqrt{2}\omega_{ew0}$ the antenna operates as a surface wave line, without radiation of the surface wave into the surrounding space. This mode of operation of the antenna is nonradiative, and it coincides with the existence mode of the surface wave on the plasma column (see Section 2).

The second mode is characterized by the presence of a surface wave component and a radiated volumetric wave component in the distribution of $E_z(r)$ (curve 2). The surface component of the wave slowly fades in the depth of the plasma, and the radiated component of the wave for the case $\omega_{Pe} = 5\omega_{ew0}$ differs in phase by more than 60° from the radiation of the metal antenna (curve 4). This is a transition mode, and it is also associated with the regime of the existence of a surface wave on the plasma column.

In the third mode (curve 3) $E_z(r)$ consists of a surface part and a volumetric wave part, but the surface wave is attenuated rapidly in the plasma and the volumetric portion is different from the MAD case (curve 4) is only 20° in phase. The difference in the phase of $E_z(r)$ for the real PAD and MAD of imperfect conductors may be less, due to the finiteness of the skin layer. This mode is linear (radiative).

The radiation patterns were plotted in the considered cases of PAD and MAD (see Fig. 6). The plasma antenna radiation patterns (curves 1-3) are normal-

ized to a metal antenna radiation pattern (curve 4), and are plotted in a rectangular coordinate system for θ values from 0° to 90° (0° coincides with the antenna axis).

As the graph shows, in the case of $n_e = 8.0 \cdot 10^{10}\,\mathrm{cm}^{-3}$, curve 1 is close to 0, i.e. when $\omega_{Pe} = \sqrt{2}\omega_{ew0}$, as noted above, the antenna does not radiate energy waves into the surrounding space, and all the energy goes to surface wave propagation along the plasma tube. In the transitional mode (curve 2) $n_e = 9.1 \cdot 10^{11}\,\mathrm{cm}^{-3}$ and $\omega_{Pe} = 5\omega_{ew0}$ the radiation pattern is smaller in amplitude than radiation pattern of the metal antenna, which means no optimum plasma antenna operating compared to MAD. The radiation pattern of the linear mode ($n_e = 3.6{\cdot}10^{12}\,\mathrm{cm}^{-3}$ and $\omega_{Pe} = 10\omega_{ew0}$, curve 3) is very close to curve 4, which implies that the plasma antenna is near to the characteristics of the metal.

5. Conclusions

We have obtained the following results by using the solution of the dispersion equation and a numerical simulation:

(1.) Three existence modes of the surface wave on an infinite plasma cylinder of finite radius.

(2.) The operation modes of a plasma asymmetric dipole antenna. They are nonradiative, transition and linear (radiative).

(3.) The relationship between the modes of the existence of a surface wave on an infinite plasma cylinder and the operation of a plasma asymmetric dipole antenna.

(4.) The dependence of the operation modes of a plasma asymmetric dipole antenna on the ratio of the plasma frequency and the electromagnetic wave frequency.

(5.) The plasma antenna characteristics in the linear mode are close to the characteristics of the metal antenna.

In addition, the models used here were verified by experimental measurements.

Acknowledgements

This work has been supported by the Russian Foundation for Basic Research (RFBR) project N14-08-31336. The authors are grateful to Professor A.A. Rukhadze and Professor A.M. Ignatov for discussions and useful comments. The measurement patterns were carried out in an anechoic chamber in the JSC Kulon Research Institute. The authors thank the management and staff of JSC Kulon Research Institute for their assistance.

References

[1] G. G. Borg, J. H. Harris, D. G. Miljak, N. M. Martin. Application of plasma columns to radiofrequency antennas. *Appl Phys Lett* **74**(22):3272, 1999. doi:10.1063/1.874041.

[2] J. P. Rayner, A. P. Whichello, A. D. Cheetham. Physical characteristics of a plasma antenna. *IEEE Trans on Plasma Science* **32**(1):269, 2004. doi:10.1109/TPS.2004.826019.

[3] I. Alexeff, T. Anderson, S. Parameswaran, et al. Experimental and theoretical results with plasma antennas. *IEEE Trans on Plasma Science* **34**(2):166, 2006. doi:10.1109/TPS.2006.872180.

[4] E. N. Istomin, D. M. Karfidov, I. M. Minaev, et al. Plasma asymmetric dipole antenna excited by a surface wave. *Plasma Physics Reports* **32**(5):388–400, 2006. doi:10.1134/S1063780X06050047.

[5] C. Liang, Y. Xu, Z. Wang. Numerical simulation of plasma antenna with fdtd method. *Chin Phys Lett* **25**(10):3712, 2008.

[6] D. Qian, D. Jun, G. Chen-Jiang, S. Lei. On characteristics of a plasma column antenna. *ICMMT* **1**:413–415, 2008. doi:10.1109/ICMMT.2008.4540404.

[7] T. Anderson. *Plasma antennas*. Artech House, Norwood, 2011.

[8] Z. Chen, A. Zhu, J. LV. Two-dimensional models of cylindrical monopole plasma antenna excited by surface wave. *WSEAS Trans on Com* **12**(2):63, 2013.

[9] N. N. Bogachev, I. L. Bogdankevich, N. G. Gusein-zade, V. P. Tarakanov. Computer simulation of plasma vibrator antenna. *Acta Polytechnica* **53**(2):1–3, 2013.

[10] V. Konovalov, G. Kuzmin, I. Minaev, O. Tikhonevich. Spectral characteristics of plasma antennas. *XLI Zvenigorod International Conference on Plasma Physics and Controlled Fusion* 2014.

[11] B. Belyaev, A. Leksikov, A. Leksikov, et al. Investigation of nonlinear behavior of plasma antenna. *Izvestiia Vysshykh Uchebnykh Zavedenii Fizika* **56**(8):88–91, 2013.

[12] M. Moisan, C. Beaudry, P. Leprince. A small microwave plasma source for long column production without magnetic field. *IEEE Transactions on Plasma Science* **3**(2):55, 1975.

[13] A. Aleksandrov, L. Bogdankevich, A. Rukhadze. *Principles of Plasma Electrodynamics*. Springer Verlach, Heidelberg, 1984.

[14] V. Tarakanov. *User's Manual for Code KARAT*. VA, Springfield, 1992.

[15] Keysight Technologies. *About EMpro*. `http://www.keysight.com/en/pc-1297143/empro`.

[16] Drude. Zur elektronentheorie der metalle. *AnndPhys* **1**:566, 1900.